Engineering Innovations
ISSN: 2813-1002, Vol. 5, pp 49-62
doi:10.4028/p-7040un

Submitted: 2022-03-22
Revised: 2022-11-29
Accepted: 2022-12-06
Online: 2023-04-19

Theoretical Study on CO_2/SO_2 Absorption Using *N*-Alkylethylenediaminium Protic Ionic Liquid

Hui Huang[1,a], Er Hua[1,2,3,b*]

[1]Chemical Science and Engineering College, China

[2]Key Laboratory of Chemical Engineering and Technology, State Ethnic Affairs Commission, including country

[3]Ningxia Key Laboratory of Solar Chemical Conversion Technology, North Minzu University, 204 Wenchang North Street, Xixia District, Yinchuan, Ningxia, 750021, China.

[a]huanghui971217@163.com, [b]huaer0101@hotmail.com

Keywords: Ethylenediaminium protic ionic liquid; CO_2; SO_2; density functional theory; hydrogen bonding

Abstract. The protic ionic liquids (PILs) comprising with *N*-2-ethylhexylethylenediaminium cation ($HEtHex^+$) and bis(trifluoromethanesulfonate)imide anion ($TFSA^-$) forming [HEtHex][TFSA] which has two amines in the polar group and available to absorbs acid gases such as CO_2 and SO_2. In order to study the CO_2/SO_2 absorption mechanism of [HEtHex][TFSA], the stable configurations of [HEtHex][TFSA]-*n*CO_2 (*n*=1, 2, 3, 4) and [HEtHex][TFSA]-*n*SO_2 (*n*=1, 2, 4, 6) are investigated using the density functional theory at the M06-2X/6-311G (*d*, *p*) level, then, the interaction energy, molecular vibration frequency, second-order perturbation energy, electron density and Laplace value are calculated and analysed for the most stable configurations. The results show that N–H···O type weak or medium hydrogen bonding are mainly formed between [HEtHex][TFSA] and CO_2/SO_2 molecules. The hydrogen bonding interaction is stronger for [HEtHex][TFSA]-*n*SO_2 comparing with [HEtHex][TFSA]-*n*CO_2 and increases with increasing the number of CO_2/SO_2 molecules.

1. Introduction

As one of the main energy sources of the present time, fossil fuels are necessary for the sustenance of human life. However, extensive usage of fossil fuels has adverse effects on the natural environment and ecological balance. The burning of fossil fuels, such as coal, oil, and natural gases, has caused a sharp increase in the amount of CO_2 and SO_2 in the atmosphere. CO_2, which is one of the most common greenhouse gases, has led to global warming and has produced a series of global climate issues today. As for SO_2, it is one of the main components of acid rain. Therefore, technology to capture CO_2 and SO_2 has become a global concern and has been attracting the attention of many researchers [1,2]. Traditional amine absorbents are volatile and not environmentally friendly. Ionic liquids (ILs), however, have many advantages [3-8] such as good thermal stability, low volatility, recyclability. This is especially true for ILs with amine groups, which have good prospects for development in the field of CO_2 and SO_2 absorption [9-11].

ILs are molten salts comprising organic or inorganic anions and organic cations with a melting point below 100 °C [12]. They are divided into two categories such as protic ionic liquids (PILs) and aprotic ionic liquids (AILs)[13]. However, with IL research, the molecular composition of ILs has become more diverse. According to statistics, there are more than 600 cations and 150 anions available to design 1018 kinds of ILs [14]. At present, most studied ILs are AILs, and they occupy the majority of ionic liquid research. In contrast, there are few publications on PILs. PILs are easy to synthesise and have strong polarity, making them suitable for absorbing and dissolving high concentrations of CO_2 and SO_2 without causing environmental pollution. Especially, protic ionic liquids comprising chelate amines should be a greater green absorbent for the waste gases.

In this study, the absorption mechanism for CO_2 and SO_2 using [HEtHex][TFSA] type PIL (Fig.1 and Scheme 1, which is experimentally synthesized and the most stable configuration of it was optimized at M06-2X/6-311G (*d*, *p*) level in our lab [15-17]) are studied using density functional

theory (DFT) [18]. Interaction energy is calculated and molecular vibration frequency, second-order perturbation energy, electron density, and Laplace value are determined. [HEtHex][TFSA] is a non-volatile PIL with two amine groups in the cationic part of the molecule. Compared with monoamine type PILs and other traditional amine absorbents, [HEtHex][TFSA] is expected as a green amine absorbent for absorbing industrial waste gases such as CO_2 and SO_2 [19,20].

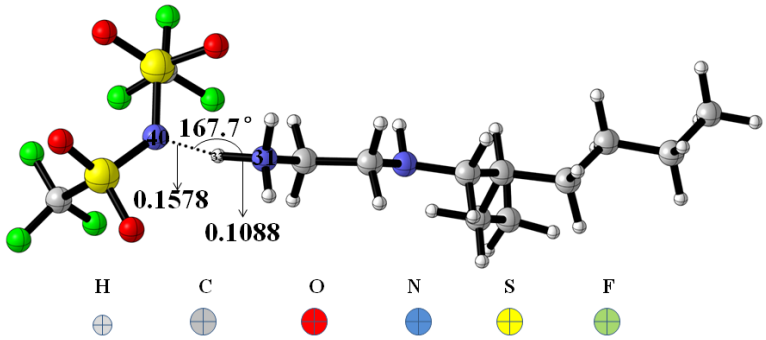

Fig.1 The three-dimensional structure of [HEtHex][TFSA], and the bonds length/nm is marked.

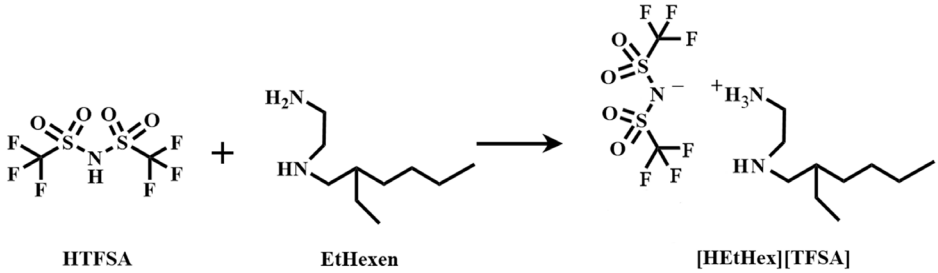

Scheme 1 The synthesis of [HEtHex][TFSA].

2. Calculation method

In this study, the configurations of [HEtHex][TFSA]-CO_2 and [HEtHex][TFSA]-SO_2 are optimised using DFT with the M06-2X functional and 6-311G (*d*, *p*) bases set. Hydrogen bonding is studied according to the results of the molecular vibration frequency, second-order perturbation energy [21], Laplace value [22], and the electron density [22] and the main charge distributions at the bond critical points (BCPs) of hydrogen bond. Moreover, reduced density gradient function analysis (GDR) [23] is utilised for analysing the strength of hydrogen bonding.

3. Results and discussion

3.1 The electrostatic potential surface.

The electrostatic potential of the monomers of [HEtHex][TFSA][15,16], CO_2 and SO_2 is calculated by the DFT with M06-2X functional and 6-311G (*d*, *p*) basis set and visualized with colors, Fig.2.

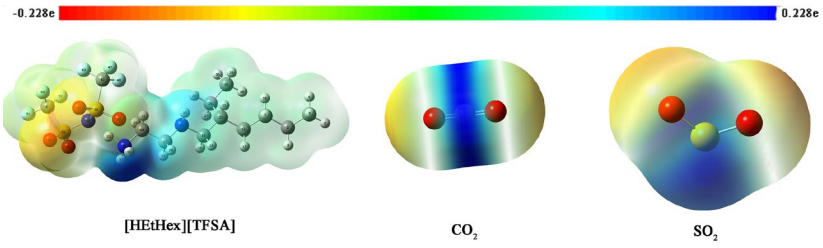

Fig.2 The electrostatic potential surface distribution for the monomers of [HEtHex][TFSA], CO_2, and SO_2.

The blue region surrounding N–H is more positive, while the yellow with red region surrounding O is more negative. Therefore, intermolecular hydrogen bonding will mainly occur between N–H in [HEtHex][TFSA] and O in SO_2 or CO_2.

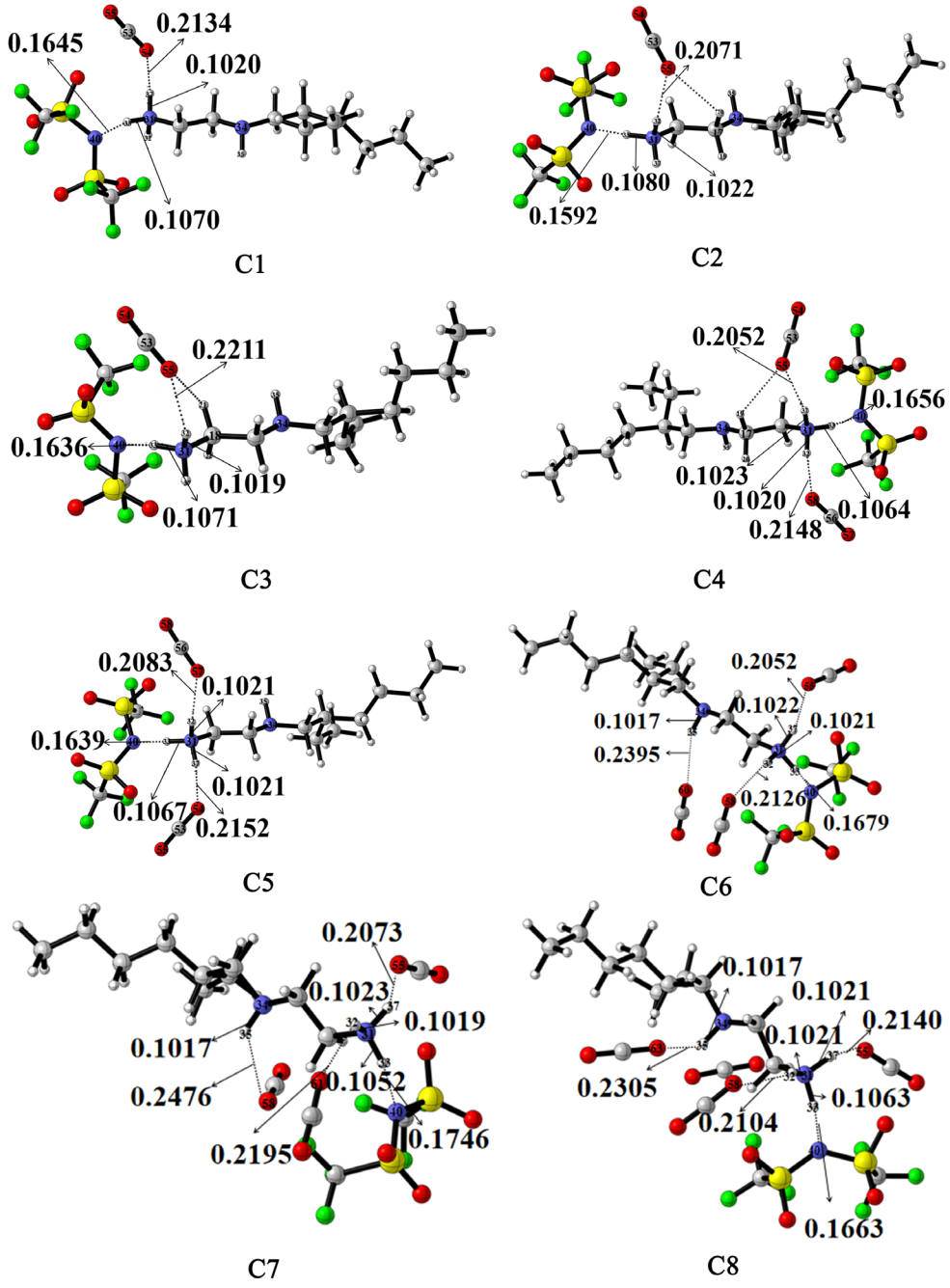

Fig.3 Optimized configurations C1-C8 of [HEtHex][TFSA]-$n$$CO_2$, and bond length/nm. C1-C3 (with $1CO_2$), C4-C5 ($2CO_2$), C6-C7 ($3CO_2$) and C8 ($4CO_2$) (red is O atom, blue is N atom, charcoal grey is C atom, light grey is H atom, yellow is S atom, green is F atom).

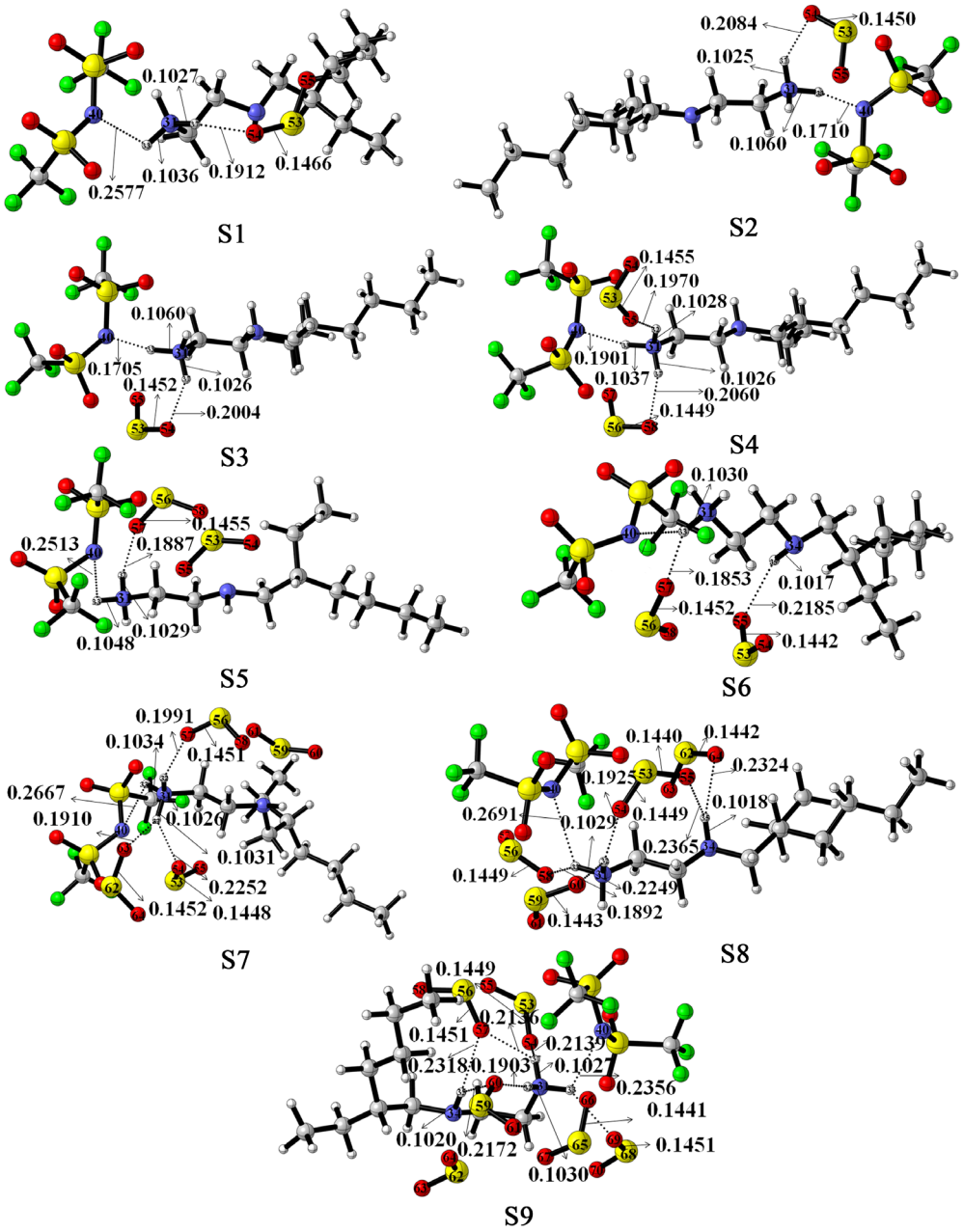

Fig. 4 Optimized configurations S1-S9 of [HEtHex][TFSA]-$n$$SO_2$, and bond length/nm, S1-S3 (with 1SO_2), S4-S6 (2SO_2), S7-S8 (4SO_2) and S9 (6SO_2). (red for O, blue N, larger grey C, smaller grey H, yellow S, green F).

The configurations C1-C8 for [HEtHex][TFSA]-$n$$CO_2$ and S1-S9 for [HEtHex][TFSA]-$n$$SO_2$ are optimized using the DFT calculation with M06-2X/6-311G (*d*, *p*) level, seen in Fig.3 and 4. And the most stable configurations of C3, C4, C6, C8 for [HEtHex][TFSA]-1, 2, 3, 4CO_2 and S1, S4, S7, S9 for [HEtHex][TFSA]-1, 2, 4, 6SO_2 are determined by the calculation of the intermolecular interaction energy using Eq.1, Eq.2, Eq.3 [24], the values are shown in Table1. The structure of [HEtHex][TFSA] with 7SO_2 is designed and tried to optimized, but it was failed.

$$\Delta E_{\text{int}} = E_{[\text{HEtHex}][\text{TFSA}]-n\text{CO}_2/\text{SO}_2} - (E_{[\text{HEtHex}][\text{TFSA}]} + nE_{\text{CO}_2/\text{SO}_2}), \tag{1}$$

$$\Delta E_0 = \Delta E_{\text{int}} + \Delta\text{ZPVE}, \tag{2}$$

$$\Delta E_0^{\text{BSSE}} = \Delta E_0 + \text{BSSE}. \tag{3}$$

ΔE_{int} is the interaction energy between molecules [HEtHex][TFSA] and $n$$CO_2$/$SO_2$, ΔE_0 is the interaction energy calculated by ZPVE correction and ΔE_0^{BSSE} is the interaction energy after the correction of ZPVE (zero-point vibration energy), and BSSE (basis set superposition error) [25]. Interaction energy increases with increasing number of $n$$CO_2$/$SO_2$ molecules. The value of ΔE_0^{BSSE} for [HEtHex][TFSA]-$n$$SO_2$ is more negative than for [HEtHex][TFSA]-$n$$CO_2$ for the same value of n. It means that intermolecular interaction is stronger for [HEtHex][TFSA]-$n$$SO_2$ than [HEtHex][TFSA]-$n$$CO_2$. This could be because of the fact that SO_2 accepts protons more readily than CO_2.

Table 1 Interaction energies for [HEtHex][TFSA]-$n$$SO_2$ and [HEtHex][TFSA]-$n$$CO_2$.

Configurations	n	ΔE_0 (kJ/mol)[a]	ΔE_0^{BSSE} (kJ/mol)[b]
[HEtHex][TFSA]		−413.0	−393.7
C1	$1CO_2$	−33.2	−27.0
C2		−34.4	−27.6
C3		−41.2	*−32.1*
C4	$2CO_2$	−70.3	*−54.2*
C5		−68.3	−52.5
C6	$3CO_2$	−91.4	*−69.9*
C7		−91.5	−64.0
C8	$4CO_2$	−120.6	*−88.0*
S1	$1SO_2$	−89.8	*−65.6*
S2		−64.1	−49.0
S3		−66.4	−50.4
S4	$2SO_2$	−130.0	*−98.7*
S5		−119.6	−79.7
S6		−110.6	−82.8
S7	$4SO_2$	−250.6	*−185.8*
S8		−221.3	−151.2
S9	$6SO_2$	−388.8	*−296.6*

a: ΔE_0: interaction energy calculated by ZPVE correction.
b: ΔE_0^{BSSE}: The interaction energy calculated by ZPVE and BSSE correction.

3.2 Infrared spectroscopy analysis. Infrared spectroscopy analysis is an important approach to evaluate the formation of the hydrogen bonds between molecules[26]. The N-H·O hydrogen bond is formed between PILs and $n$$CO_2$/$SO_2$; further, the bond length of H··O is in the range of 0.10–0.27 nm and can be classified as a weak or medium strength hydrogen bond. Table 2 summarizes that the vibration frequency of 31N-33H between the cation and anion of PILs undergoes a blue shift after combining with CO_2/SO_2, and the change in its value increases with the number of gas molecules. This change in value is much greater for [HEtHex][TFSA]-$n$$SO_2$ than it is for [HEtHex][TFSA]-$n$$CO_2$. Meanwhile, for N-H in N-H···O bonding, the change in frequency and bond length is nearly zero for CO_2, while a greater red shift (Δv 77 − 203 cm^{-1}) is observed for SO_2. This result implies that intermolecular hydrogen bonding between PILs and gas molecules is much stronger when binding with SO_2 than it is with CO_2. In addition, when bonding with CO_2, the intermolecular interaction is small. This could be because SO_2 accepts protons more easily than CO_2.

Table 2 The frequency (ν/cm^{-1}) and bond length (nm) changes for N-H before and after the absorption of CO_2/SO_2

Configurations	n	N—H Bond	ν/cm^{-1}	$\Delta\nu$/cm^{-1}	r/nm	Δr/nm
[HEtHex][TFSA]		31N—32H	3461		0.1022	
		31N—33H	2343		0.1088	
		31N—37H	3461		0.1019	
		34N—35H	3525		0.1017	
C2	1CO_2	31N—33H	2452	−109	0.1080	−0.0008
		31N—32H	3472	−11	0.1022	0.0000
		55O—32H			0.2071	
C4	2CO_2	31N—33H	2729	−386	0.1064	−0.0024
		31N—32H	3473	−13	0.1020	−0.0002
		31N—37H	3474	−13	0.1023	0.0003
		55O—37H			0.2052	
		58O—32H			0.2148	
C6	3CO_2	31N—33H	2815	−472	0.1059	−0.0029
		31N—32H	3437	+23	0.1021	−0.0001
		31N—37H	3437	+23	0.1022	0.0003
		34N—35H	3538	−13	0.1017	0.0000
		58O—32H			0.2126	
		60O—35H			0.2395	
		55O—37H			0.2052	
C8	4CO_2	31N—33H	2739	−396	0.1064	−0.0024
		31N—32H	3485	−25	0.1021	−0.0001
		31N—37H	3485	−25	0.1021	0.0002
		34N—35H	3531	−7	0.1017	0.0000
		58O—32H			0.2104	
		63O—35H			0.2305	
		55O—37H			0.2140	
S1	1SO_2	31N—33H	3257	−913	0.1036	−0.0052
		31N—37H	3258	+203	0.1027	0.0008
		54O—37H			0.1912	
S6	2SO_2	31N—33H	3369	−1025	0.1030	−0.0059
		34N—35H	3547	−22	0.1017	0.0000
		57O—33H			0.1853	
		55O—35H			0.2185	
S8	4SO_2	31N—33H	3383	−1040	0.1029	−0.0060
		31N—32H	3383	+77	0.1029	0.0007
		34N—35H	3537	−12	0.1018	0.0001
		58O—33H			0.1892	
		54O—32H			0.1925	
		60O—32H			0.2249	
		55O—35H			0.2365	
		64O—35H			0.2324	

		31N—33H	3378	−1104	0.1027	−0.0061
		31N—32H	3378	+82	0.1030	0.0008
		31N—37H	3378	+82	0.1026	0.0006
		34N—35H	3520	+5	0.1020	0.0003
S9	$6SO_2$	57O—35H			0.2318	
		57O—37H			0.2136	
		60O—35H			0.2172	
		60O—32H			0.1903	
		54O—37H			0.2139	
		69O—33H			0.2237	

[a] $\Delta v = v_{[HEtHex][TFSA]} - v_{[HEtHex][TFSA]\text{-}so2/co2}$; [b] $\Delta r = r_{[HEtHex][TFSA]\text{-}so2/co2} - r_{[HEtHex][TFSA]}$

3.3 Natural population analysis. The charge distribution in [HEtHex][TFSA]-$n$$CO_2$/$SO_2$ is calculated by DFT with the M06-2X functional and 6-311G (*d*, *p*) basis set, the data are listed in Table 3 and Table 4. Electron density decreases on the H atom of N–H and increases on the hydrogen bond acceptor atom, O. For example, by surrounding the hydrogen bonding of 31N–37H···54O in S1 with $1SO_2$, the charge in 54O becomes more negative (from –0.786 e to –0.957 e) and the H atom becomes positive (from 0.415 to 0.455 e). For the 31N–32H···55O in C1 with $1CO_2$, the charge on 55O becomes more negative, (from –0.518 e to –0.606 e) and the H atom becomes positive (from 0.428 to 0.435 e). This suggests that a stronger hydrogen bond is formed between [HEtHex][TFSA] and $n$$CO_2$/$SO_2$ molecules. This result is consistent with the result of infrared spectroscopy analysis.

Table 3 Selected partial charges/e from NPA of [HEtHex][TFSA]-$n$$CO_2$.

Configurations	n	Bonds	Atoms					
			31N	34N	32H	35H	37H	O
CO_2		C–O						−0.518
[HEtHex][TFSA]		31N–33H	−0.736					
		31N–32H			0.428			
		34N–35H		−0.686		0.350		
		31N–37H					0.415	
C2	$1CO_2$	31N–32H···55O	−0.740		0.435			−0.606
C4	$2CO_2$	31N–37H···55O	−0.740				0.440	−0.601
		31N–32H···58O	−0.740		0.429			−0.601
C6	$3CO_2$	31N–37H···55O	−0.740				0.439	−0.600
		31N–32H···58O	−0.740		0.431			−0.579
		34N–35H···60O		−0.691		0.359		−0.577
C8	$4CO_2$	31N–37H···55O	−0.738				0.435	−0.595
		31N–32H···58O	−0.738		0.433			−0.592
		34N–35H···63O		−0.700		0.361		−0.568

Table 4 Selected partial charges/e by NPA of [HEtHex][TFSA]-$n$$SO_2$.

Configurations	n	Bonds	Atoms						
			31N	34N	32H	33H	35H	37H	O
SO_2		S–O							−0.786
[HEtHex][TFSA]		31N–33H	−0.736			0.489			
		31N–32H			0.428				
		34N–35H		−0.686			0.350		
		31N–37H						0.415	
S1	1SO_2	31N–37H···54O	−0.735					0.455	−0.957
S6	2SO_2	31N–33H···57O	−0.725			0.467			−0.891
		34N–35H···55O		−0.702			0.377		−0.816
S8	4SO_2	31N–33H···58O	−0.743			0.477			−0.868
		31N–32H···60O	−0.743		0.471				−0.821
		31N–32H···54O	−0.743		0.471				−0.883
		34N–35H···64O		−0.696			0.376		−0.810
S9	6SO_2	31N–37H···54O	−0.781					0.474	−0.871
		31N–37H···57O	−0.781					0.474	−0.887
		31N–32H···60O	−0.781		0.467				−0.900
		34N–35H···64O		−0.696			0.438		−0.978
		31N–32H···66O	−0.781		0.467				−0.806
		31N–33H···69O	−0.781			0.473			−0.891

The second-order perturbation stabilization energy, $E^{(2)}$ (kJ/mol), which is described by Eq.4 as follows [21], corresponding to the LP (O) donor → σ* (N–H) acceptor interaction is calculated for the configurations of C2, C4, C6, C8 and S1, S6, S8, S9 with the strongest hydrogen bond, the data are listed in Table 5.

$$E^{(2)} = \frac{q_i F(i,j)^2}{\varepsilon_i - \varepsilon_j} . \tag{4}$$

Among them, (i) and (j) represent the donor and acceptor orbitals, respectively, the qi is the donor orbital occupancy, ε_i and ε_j are the diagonal elements (orbital energies), and (F(i, j)) is the off-diagonal or coupling NBO Fock matrix element. As shown in Table 5, $E^{(2)}$ and $E^{(2)}_{sum}$ values of LP(O)→BD*(N–H) for [HEtHex][TFSA]-$n$$SO_2$ are much larger than those for [HEtHex][TFSA]-$n$$CO_2$, which means that the hydrogen bonding between [HEtHex][TFSA] and $n$$SO_2$ is much stronger than that between [HEtHex][TFSA] and $n$$CO_2$. For example, in the case with 2SO_2, $E^{(2)}_{sum}$ is 47 kJ/mol and the value is almost twice that of the case with 2CO_2, 29 kJ/mol. The strength of hydrogen bonding is strong for [HEtHex][TFSA]-SO_2 and medium for [HEtHex][TFSA]-CO_2, that are described in Table 7.

Meanwhile, the $E^{(2)}_{sum}$ value for C6 with 3CO_2 (34 kJ/mol) is larger than that for C8 with 4CO_2 (27 kJ/mol). At the same time, for [HEtHex][TFSA] with 6SO_2, the $E^{(2)}_{sum}$ value reaches a maximum of 135 kJ/mol. This means that one [HEtHex][TFSA] molecule becomes saturated when bonding with three CO_2 molecules or six SO_2 molecules.

Table 5 The second-order stabilization energies $E^{(2)}$ (kJ/mol) at BCP of [HEtHex][TFSA]-$n$$CO_2$/$n$$SO_2$.

Configurations	n	Charge transfer	$E^{(2)a}$	$E^{(2)}{}_{sum}{}^b$
C2	$1CO_2$	LP(O55)→BD*(N31-H32)[c]	16	17
C4	$2CO_2$	LP(O55) →BD*(N31-H37)	21	29
C6	$3CO_2$	LP(O55) →BD*(N31-H37) LP(O58) →BD*(N31-H32)	19 11	34
C8	$4CO_2$	LP(O55) →BD*(N31-H37) LP(O58) →BD*(N31-H32)	10 11	28
S1	$1SO_2$	LP(O54) →BD*(N31-H37)	29	29
S6	$2SO_2$	LP(O55) →BD*(N34-H35) LP(O57→BD*(N31-H33)	10 37	47
S8	$4SO_2$	LP(O54) →BD*(N31-H32) LP(O58) →BD*(N31-H33) LP(O60) →BD*(N31-H32)	31 46 14	108
S9	$6SO_2$	LP(O54) →BD*(N31-H37) LP(O57) →BD*(N31-H37) LP(O60) →BD*(N31-H32) LP(O60) →BD*(N34-H35) LP(O69) →BD*(N31-H33)	22 17 45 16 15	135

a: ③ $E^{(2)}$<30, 30 < $E^{(2)}$< 150, $E^{(2)}$> 150 kJ/mol are weak, medium and strong hydrogen bond, respectively.
$E^{(2)}$ values less than 10 kJ/mol have been omitted.
b: $E^{(2)}{}_{sum}$ is the sum of $E^{(2)}$ of the BCP in the configuration.
c: LP is lone pair, and BD* is bond donor.

3.5 The theory of the atoms in molecules. The topological properties of the electron density scalar field can be obtained from the theory of atoms in molecules and used to describe the characteristic of bonding between atoms. The electron density [22] (ρ_c, a.u.), Laplace value ($\nabla^2\rho_c$, a.u.) [22] for [HEtHex][TFSA]-$n$$CO_2$/$SO_2$ are calculated by DFT theory with M06-2X/6-311G(d, p) and the data are listed in Table 6. The hydrogen bonding energy, E_{HB} (kJ/mol) is calculated using Eq. 5. $V_{(r)}$ stands for electron potential density at BCP.

$$E_{HB} = (V_{(r)} /(-2)) \times 627.15 \quad (5)$$

$\nabla^2\rho_c$ at BCPs are positive for all of the configurations, E_{HB} values are in the range of 8~34 kJ/mol. Among them, the maximum E_{HB} of the hydrogen bonding in [HEtHex][TFSA]-$n$$SO_2$ is as high as 34 kJ/mol, while that in the case of CO_2 is only 17 kJ/mol. This means hydrogen bonding is stronger for [HEtHex][TFSA]-$n$$SO_2$ than for [HEtHex][TFSA]-$n$$CO_2$. The value of ρ_c is also in an agreement with the result of E_{HB} values. This could be because of the fact that SO_2 accepts protons more readily than CO_2.

The $\rho_{c(sum)}$ of [HEtHex][TFSA] with $1SO_2$, $2SO_2$, $4SO_2$, $6SO_2$ are 0.0265, 0.0452, 0.0890, 0.1005 and with $1CO_2$, $2CO_2$, $3CO_2$, $4CO_2$ are 0.0175, 0.0335, 0.0428, 0.0441, respectively. This means that intermolecular hydrogen bonding increases with an increasing number of SO_2/CO_2 molecules, which agrees with the result of the second-order perturbation energy study.

Meanwhile, the value of ρ_c and E_{HB} is in the region of strong hydrogen bonding for [HEtHex][TFSA]-$n$$SO_2$ and medium for [HEtHex][TFSA]-$n$$CO_2$, respectively as shown in Table 7 and Fig.5.

Table 6 The values of electron density, ρ_c (a.u.), Laplacian of electron density, $\nabla^2\rho_c$(a.u.), hydrogen bonding energy, E_{HB} (kJ/mol) at bond critical point of [HEtHex][TFSA]-nCO$_2$/nSO$_2$.

Configurations	n	BCPs	$\nabla^2\rho_c$	E_{HB}	ρ_c	$\rho_{c(sum)}$[a]
C2	1CO$_2$	55O···32H–31N	0.076	*17*	0.018	0.018
		58O···32H–31N	0.068	15	0.016	
C4	2CO$_2$	55O···37H–31N	0.077	*17*	0.018	0.034
		57O···32H–31N	0.074	16	0.017	
C6	3CO$_2$	55O···37H–31N	0.078	*17*	0.018	0.043
		58O···32H–31N	0.069	15	0.016	
		60O···35H–34N	0.033	8	0.009	
C8	4CO$_2$	58O···32H–31N	0.068	15	0.016	0.044
		55O···37H–31N	0.071	16	0.016	
		63O···35H–34N	0.045	11	0.012	
S1	1SO$_2$	31N···37H–54O	0.114	*30*	0.026	0.027
S6	2SO$_2$	31N···33H–57O	0.121	*34*	0.029	0.045
		34N···35H–55O	0.060	15	0.016	
S8	4SO$_2$	34N···35H–64O	0.041	10	0.012	0.089
		34N···35H–55O	0.039	10	0.011	
		31N···32H–54O	0.111	*27*	0.025	
		31N···32H–60O	0.051	12	0.014	
		31N···33H–58O	0.114	*30*	0.027	
		34N···35H–57O	0.049	13	0.013	
S9	6SO$_2$	31N···37H–57O	0.075	17	0.017	0.101
		34N···35H–60O	0.060	15	0.016	
		31N···32H–60O	0.106	*27*	0.025	
		31N···33H–69O	0.050	12	0.013	
		31N···37H–54O	0.066	15	0.016	

a: $\rho_{c\ (sum)}$ is the sum of the ρ_c values of the main hydrogen bonding in the configuration.

Table 7 Suggested strength for hydrogen bonds[27-29] and corresponding value calculated for [HEtHex][TFSA]- nSO$_2$/CO$_2$ in this study, among them, H···Y and H–X are corresponded to H···O and H–N, respectively.

Parameters	Weak	Medium	Strong	[HEtHex][TFSA]-nSO$_2$	Strength	[HEtHex][TFSA]-nCO$_2$	Strength
	Weak ionic dispersion	Ionic	Covalent				
H···Y (nm)	> 0.22	0.15–0.22	0.12–0.15	0.10–0.24	Medium	0.10–0.25	Weak or Medium
X–H *vs.* H···Y	X–H << H···Y	X–H < H···Y	X–H ≈ H···Y	N–H < H···O	Medium	N–H < H···O	Medium
ρ_c (a.u.)	0.02–0.002	0.02–0.05	> 0.05	0.027–0.101	Medium	0.018–0.044	Weak
$E^{(2)}$ (kJ·mol^{-1})	< 29	29–150	> 150	29-135	Medium	17-34	Weak
E_{HB} (kJ·mol^{-1})	< 16	16–62	62–167	10-34	Medium	8–17	Weak

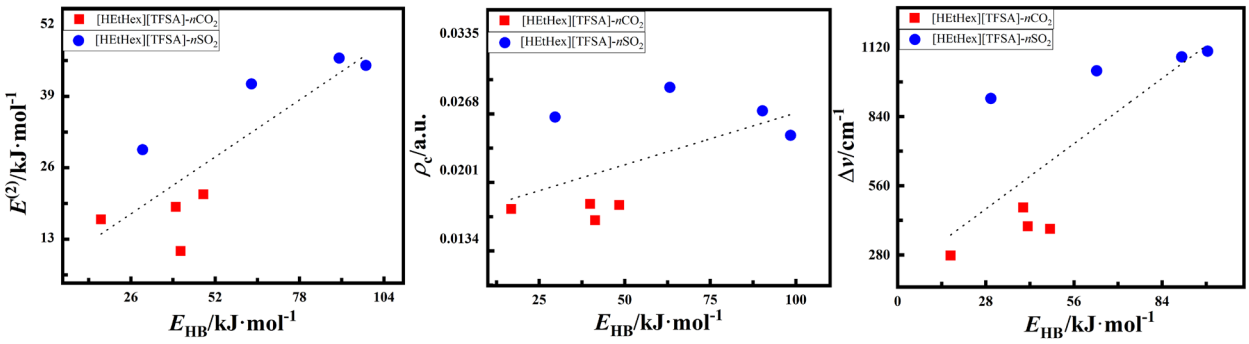

Fig.5 The second-order stabilization energies, $E^{(2)}$ (kJ/mol), electron density, ρ_c (a.u.), and the change in vibrational frequency, ν(cm^{-1}) as a function of hydrogen bonding energy, E_{HB} (kJ/mol) for N—H···O hydrogen bonds in [HEtHex][TFSA]-nCO$_2$ (n=1, 2, 3, 4) and [HEtHex][TFSA]-nSO$_2$ (n=1, 2, 4, 6).

3.6 The analysis of RDG. To describe the strength of hydrogen bonding between [HEtHex][TFSA] and $n$$SO_2$/$CO_2$, a scatter diagram and colour-filled reduced density gradient (RDG) isosurface map is drawn and shown in Fig.6 and 7. The spurs on the left, in the middle, and on the right in Fig.6a and Fig.7a correspond to hydrogen bonding, van der Waal forces, and nonbonded overlap, respectively, and also correspond to the blue, green, and red regions in Fig.6b c and Fig.7b c, respectively. The denser spur on the left means stronger hydrogen bonding between [HEtHex][TFSA] and $n$$SO_2$/$n$$CO_2$. In contrast, the density of the spur increases with an increasing number of SO_2/CO_2 molecules bonding with [HEtHex][TFSA], with a denser spur in the case of SO_2 and a sparser spur for CO_2. This result, which shows that the absorption ability of [HEtHex][TFSA] is better for SO_2 than CO_2, is consistent with the result of AIM and NBO analyses.

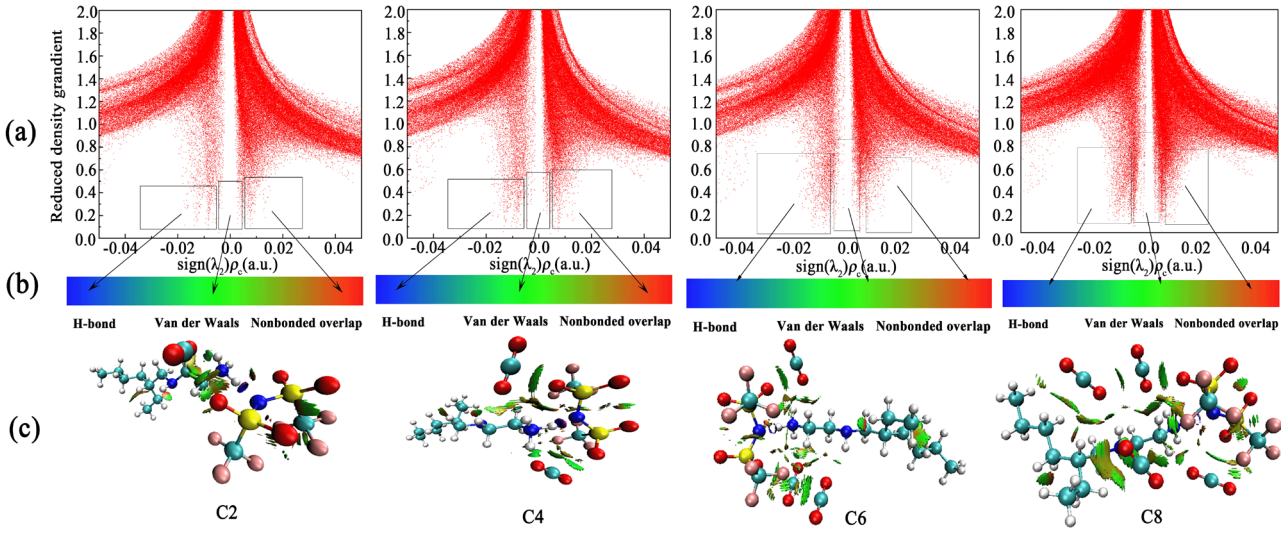

Fig.6 The scatter diagram and color-filled RDG isosurface map of [HEtHex][TFSA]-$n$$CO_2$ (n=1, 2, 3, 4)

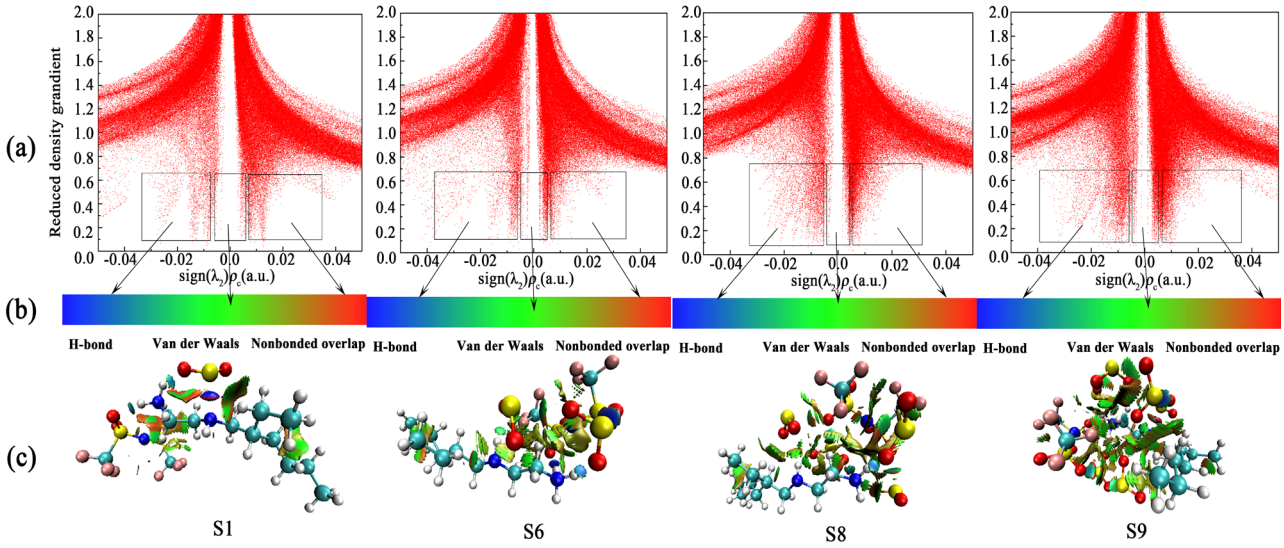

Fig.7 The scatter diagram and color-filled RDG isosurface map of [HEtHex][TFSA]-$n$$SO_2$ (n=1, 2, 4, 6).

4. Conclusion

The absorption of CO_2/SO_2 using the chelating PILs composed of *N*-2-ethylhexylethylenediaminium cation and TFSA anion ([HEtHex][TFSA]) was invested at the electronic and molecular level using M06-2X/6-311G (*d*, *p*) of DFT calculation. The N–H···O interactions between [HEtHex][TFSA] and CO_2/SO_2 were determined and used for classification of

the H-bonds in the structure of [HEtHex][TFSA]-$n$$CO_2$/$SO_2$. The total H-bond energy of [HEtHex][TFSA]-$n$$CO_2$ (or $n$$SO_2$) increased with the number of gas molecules. AIM analyses and NBO data showed that the H-bond energies for the interactions in the structures of PILs-$n$$SO_2$ are larger than those for PILs-$n$$CO_2$. The PILs combined with SO_2 have H-bond energies within the range of 10–34 kJ/mol, $E^{(2)}$ values within the range of 29–135 kJ/mol, H···O bond lengths within the range of 0.10–0.24 nm, and ρ_c within the range of 0.027–0.101 a.u. At the BCPs, in contrast, these values for PILs-$n$$CO_2$ are within the range of 8–17 kJ/mol, 17–34 kJ/mol, 0.10–0.25 nm, and 0.018–0.044 nm, respectively. These values enabled the classification of the H-bonds for PILs-$n$$SO_2$ as strong and those for PILs-$n$$CO_2$ as weak H-bonds. This could be because of the fact that SO_2 accepts protons more readily than CO_2.

Supplementary Material

See Supporting Information for the complete original vibrational frequency, charge distribution, second-order perturbation stabilization energy, and electron density data.

Acknowledgements

This work was financially supported by the Natural Science Foundation of the Ningxia Hui Autonomous Region (Project Number: 2021AAC03181), the Graduate Innovation Program of North Minzu University (Project Number: YCX21134) and the Scientific Research Foundation for Returned Scholars of Ministry of Education (Project Number: [2013] No. 693). We are grateful to Miss Zheng Liu for assisting in the synthesis of the PILs and investigating their properties in a previous study.

References

[1] C.M. Wang, X.Y. Luo, X. Zhu, G.K. Cui, D. Jiang, D.S. Deng, L. Haoran, D. Sheng, The strategies for improving carbon dioxide chemisorption by functionalized ionic liquids, J. RSC Advances. 36 (3) (2013) 15518–15527.

[2] C.H. Yu, C.H. Huang, C.S. Tan, A review of CO_2 capture by absorption and adsorption, Aerosol Air Qual Res. 12 (5) (2012) 745–769.

[3] P.A. Hunt, Quantum chemical modeling of hydrogen bonding in ionic liquids, Chem. Soc. Rev. 44 (2015) 1257–1288.

[4] K.S. Egorova, E.G. Gordeev, V.P. Ananikov, Biological activity of ionic liquids and their application in pharmaceutics and medicine, Chem. Rev. 117 (2017) (10) 7132-7189.

[5] R.L. Vekariya, A review of ionic liquids: applications towards catalytic organic transformations, J. Mol. Liq. 227 (2017) 44–60.

[6] S.J. Zeng, X.P. Zhang, L. Bai, X.C. Zhang, H. Wang, J.J. Wang, D. Bao, M.D. Li, X.Y. Liu, S.J. Zhang, Ionic liquid-based CO_2 capture systems: structure, interaction and process, Chem. Rev. 117 (2017) (14) 9625–9673.

[7] V. Plechkovan, K.R. Seddon, Applications of ionic liquids in the chemical industry, Chem. Soc. Rev. 37 (2008) 123–150.

[8] P. Wasserscheid, T. Welton, Ionic liquids in synthesis, Wiley-VCH, New York, 2007.

[9] D. Fu, P. Zhang, L.X. Du, Progress in CO_2 capture using amino acid ionic liquid promoted amine aqueous solutions, Energy Sci. Eng. 30 (2014) (3) 1–4.

[10] S. Saravanamurugan, A.J. Kunov-Kruse, R. Fehrmann, A. Riisager, Amine-functionalized amino acid-based ionic liquids as efficient and high-capacity absorbents for CO_2, Chem. Sus. Chem. 7 (3) (2014) 897–902.

[11] I. Niedermaier, M. Bahlmann, C. Papp, C. Kolbeck, W. Wei, S.K. Calerón, M. Grabau, P.S. Schulz, P. Wasserscheid, H.P. Steinrück, F. Maier, Carbon dioxide capture by an amine functionalized ionic liquid: fundamental differences of surface and bulk behavior, J. Am. Chem. Soc. 136 (1) (2014):436-41.

[12] J.S. Wilkes, A short history of ionic liquids—from molten salts to neoteric solvents, Green Chemistry. 4(2) (2002) 73-80.

[13] T.L. Greaves, C.J. Drummond, Protic ionic liquids: properties and applications. Chem. Rev. 108 (1) (2008) 206-237.

[14] A.R. Katritzky, R. Jain, A. Lomaka, R. Petrukhin, M. Karelson, A.E. Visser, R.D. Rogers, Correlation of the melting points of potential ionic liquids (imidazolium bromides and benzimidazolium bromides) using the CODESSA program. J Chem Inf Model. 42 (2) (2002) 225-231.

[15] Z. liu, R. Liu, E. Hua, J.L. Yi, Water effects on physicochemical properties of protic ionic liquid with N-hexylamine as cation and bis(trifluoromethylsulfonyl) imide as anion, Chem. Eng. J. 40 (4) (2021) 2270-2277.

[16] X.C. Zhang, Y. Xu, E. Hua, Hydrogen bonding study on protic ionic liquids composed of N-alkylethylenediaminium cations with bis(trifluoromethylsulfonyl)imideanion, Journal of Shihezi University (Natural Science). 38 (5) (2020) 540-547.

[17] Y. Zhao, D.G. Truhlar, The M06 suite of density functionals for main group thermochemistry, thermochemical kinetics, noncovalent interactions, excited states, and transition elements: two new functionals and systematic testing of four M06-class functionals and other functionals, Theor Chem Acc. 120 (1) (2008) 215-241.

[18] R.G. Parr, W. Yang, Density-functional theory of atoms and molecules, Oxford University Press, New York, 1989.

[19] E.D. Bates, R.D. Mayton, I. Ntai, J.H. Davis, CO_2 capture by a task-specific ionic liquid. J. Am. Chem. Soc. 124 (6) (2002) 926-7.

[20] W. Wu, B.X. Han, H.X. Gao, Z.M. Liu, T. Jiang, J. Huang, Desulfurization of flue gas: SO_2 absorption by an ionic liquid. Angew. Chem. Int. Ed. 43 (18) (2004) 2415-7.

[21] Y WU, T T ZHANG, N YU, Interaction between 1-Ethyl-3-Methyl-Imidazolium cation and asparagine anion, ACTA PHYS-CHIM SIN. 25 (08) (2009) 1689-1696.

[22] R.F.W. Bader, Atom in Molecules: A Quantum Theory. Oxford University Press, Clarendon Press, Oxford, 1990.

[23] J.M. Campo, J.L. Gázquez, R.J. Alvarez-Mendez, A. Vela, The reduced density gradient in atoms. Int. J. Quantum Chem. 112 (22) (2012) 3594-3598.

[24] H. Roohi, K. Ghauri, Exploring physicochemical properties of the nanostructured Tunable Aryl Alkyl Ionic Liquids (TAAILs). J. Mol. Liq. 209 (2015) 14-24.

[25] S.F. Boys, F. Bernardi, The calculation of small molecular interactions by the differences of separate total energies: some procedures with reduced errors, J. Mol. Phys. 19 (1970) 553–566.

[26] H. Watanabe, H. Doi, S. Saito, M. Matsugami, K. Fujii, R. Kanzaki, Y. Kameda, Y. Umebayashi, Hydrogen bond in imidazolium based protic and aprotic ionic liquids, J. Mol. Liq. 217 (2016) (217) 35–42.

[27] J.A. George. An introduction to hydrogen bonding, Oxford University Press,1997.

[28] A.E. Reed, L.A.F. Curtiss, Weinhold intermolecular interactions from a natural bond orbital, donor-acceptor viewpoint. Chem. Rev. 88(6) (1988) 899–926.

[29] P.A. Hunt, C.R. Ashworth, R.P. Matthews R. Hydrogen bonding in ionic liquids, Chem. Soc. Rev. 44 (5) (2015) 1257-1288.